Agricultural Water Management 299 (2024) 108896

Contents lists available at ScienceDirect

Agricultural Water Management

journal homepage: www.elsevier.com/locate/agwat

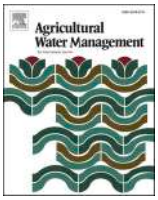

Optimizing variable rate irrigation using model and satellite-based dynamic prescription maps

Chiara Corbari [a,*], Davide Gabrieli [b], Lorenzo Furlan [c], Jacopo Furlanetto [b], Drazen Skokovic [d], Josè Sobrino [d], Francesco Morari [a]

[a] Politecnico di Milano, Milan, Italy
[b] Department of Agronomy Food Natural resources Animals and Environment, University of Padua, Italy
[c] Agenzia Veneta per l'innovazione nel Settore primario, Italy
[d] Universitat de Valencia, Spain

ARTICLE INFO

Handling editor: J.E. Fernández

Keywords:
Variable rate irrigation
Dynamic prescription maps
Energy-water balance model
Remote sensing
Water use efficiency

ABSTRACT

Variable rate irrigation is usually based on prescription maps delineated according to a static approach. Irrigation rate and timing are optimized by sensor and/or models applied within homogenous zones whose spatial distribution is kept constant during the crop season. The objective of this study was to develop a procedure based on the combination of the crop-energy-water balance model FEST-EWB-SAFY with satellite data of vegetation variables and land surface temperature (LST) to generate dynamic irrigation prescription maps. The FEST-EWB-SAFY model couples the energy-water balance FEST-EWB, which allows computing continuously in time and distributed in space soil moisture and evapotranspiration, and the SAFY, a simple model for yield prediction and plant development. The model was tested in a 17.6 ha field cultivated with soybean in 2022 at Ceregnano (Italy). Irrigation was provided by a lateral move irrigation machine, equipped with a precision irrigation system with lateral resolution of 34 m. The model was pixelwise calibrated with satellite LST (RMSE 1.3 °C) and leaf area index (RMSE 0.45) as well as local measured soil moisture at 10 cm and 50 cm depth (RMSE 0.04). Four dynamic prescription maps were generated, calculating the pixel-by-pixel difference between the field retention capacity and the daily average of the 50-cm soil moisture profile computed by the FEST-EWB-SAFY. Dynamic variable rate irrigation was compared with a conventional irrigation system according to an experimental block design with three replicates and evaluated in terms of crop yield, irrigation volumes and irrigation water productivity (WP). The computed dynamic maps captured the crop water requirement variability originated by the interaction of ET, soil properties and field management. Compared with conventional system, there was a significant increase in WP, but not in crop yield. These results confirm that model-based dynamic prescription maps could be used to optimize variable irrigation in highly spatio-temporal dynamic cropping systems.

1. Introduction

Agriculture is a significant user of freshwater, accounting for approximately 70% of the total consumption, with localized peaks of up to 80% observed in the Mediterranean area (FAO, 2018). Furthermore, there is a significant concern regarding the inefficient utilization of water within the agricultural sector. As other sectors compete for access to water resources, it is anticipated that the situation will significantly deteriorate in the coming decades, as suggested by Ingram (2011) and Wada et al. (2011). Therefore, ensuring a rational and efficient use of water in agriculture is critical to satisfy the increasing food demands of the global population (Alexandratos et al., 2012).

Recent studies have shown that variable rate irrigation (VRI) is a promising technique for improving water management by reducing over irrigation and minimizing runoff and deep percolation. This, in turn, leads to improved water use efficiency and higher crop yields (Koech and Langat, 2018; Vellidis et al., 2016; Liakos et al., 2017).

Indeed, VRI offers the flexibility to provide precise and varying amounts of water along center pivots (Dukes and Perry, 2006; Chávez et al., 2010; O'Shaughnessy et al., 2016) and, more recently, drip lines (Jashami et al., 2021; Ortuani et al., 2019).

VRI operations rely on prescription maps, which consist of

* Correspondence to: Politecnico di Milano, Piazza Leonardo da Vinci 32, 20133, Milan, Italy.
E-mail address: chiara.corbari@polimi.it (C. Corbari).

https://doi.org/10.1016/j.agwat.2024.108896
Received 26 January 2024; Received in revised form 14 May 2024; Accepted 21 May 2024
Available online 24 May 2024

instructions to the mechanic system applying different irrigation volumes to each irrigation management zone (IMZs). Prescription maps are usually generated at the start of the growing season, taking into account the field variability in terms of crop yield, soil properties, topography, apparent soil electrical conductivity, etc. However, static prescription maps have limitations as they overlook the spatiotemporal variability of crop water stress throughout the growing season due to meteorological variability or crop disease (Falkenberg et al., 2007).

Recently, VRI systems have been used in combination to continuos measurements of soil moisture sensors, leaf water potential or thermal infrared information to determine time variable appropriate irrigation rates for different IMZs (Gobbo et al., 2019; Vellidis et al., 2013; Meron et al., 2010; Chastain et al., 2016; Snider et al., 2015).

VRI scheduling might be based also on crop evapotranspiration (ET). This has been traditionally calculated using the FAO reference evapotranspiration (ET0) and a crop coefficient (Allen et a., 1998), without taking into account potential spatial variations in ET linked to field areas with limited water or nutrient supply (Allen et al., 2007; Calera Belmonte et al., 2017). Numerous studies have utilized energy balance techniques (Bastiaanssen et al., 1998; Su, 2002; Norman et al., 1995; Teixeira et al., 2009; Papadavid et al., 2013; Bastiaanssen et al., 2005; Grosso et al., 2018) to compute maps of evapotranspiration from regional to field scales, in combination to satellite land surface temperature images from Landsat or MODIS.

However, one of the main issue, which limits their use in operative water management application at farm level, is related to the current temporal and spatial resolution of thermal infrared data, being the highest spatial resolution of Landsat data (60–100 m) available every 8–16 days (Anderson et al., 1997; Alexandridis et al., 2009). Furthermore, the spatial resolution of ET maps generated through remote sensing-based energy balance techniques often does not align with the spatial resolution required for VRI. Some techniques have been tested to overcome these low resolutions limititations as data fusion (Gao et al., 2017; Guzinski and Nieto, 2019), data modeling integration (Corbari et al., 2020; Vazifedoust et al., 2009), and temporal integration (Brutsaert and Sugita, 1992; Anderson et al., 2011).

Thus, although these models have been widely used to map ET, their application for scheduling irrigation has been limited (Knipper et al., 2019; Gobbo et al., 2019; Xue et al., 2022; Bastiaanssen and Ali, 2003).

Addressing this gap of the temporal continuity by providing information at pixel scale (compatible with the irrigated footprint area of each sprinkler on a daily scale) to the VRI system, the objective of this paper is to develope a procedure, based on the combination of the crop-energy-water balance model FEST-EWB-SAFY (Corbari et al., 2022) with remote sensing data of vegetation variables and land surface temperature, to generate dynamic irrigation prescription maps. The crop-energy-water balance FEST-EWB-SAFY model couples the distributed energy-water balance FEST-EWB (Corbari et al., 2011), which allows computing continuously in time and distributed in space both soil moisture and effective evapotranspiration fluxes independently of thermal infrared data input, and the SAFY (simple model for yield prediction and plant development) (Duchemin, et al., 2008). This procedure has been preliminarly tested in a 17.6-ha field cultivated with soybean in 2022 in Northern Italy, equipped with lateral-move irrigation systems.

2. Study area and data

The study site was a 17.6-ha field located in the lower zone of the Po Valley, at Ceregnano farm (45° 34.9650 N 12° 11.5140 E, 6 m a.s.l.)

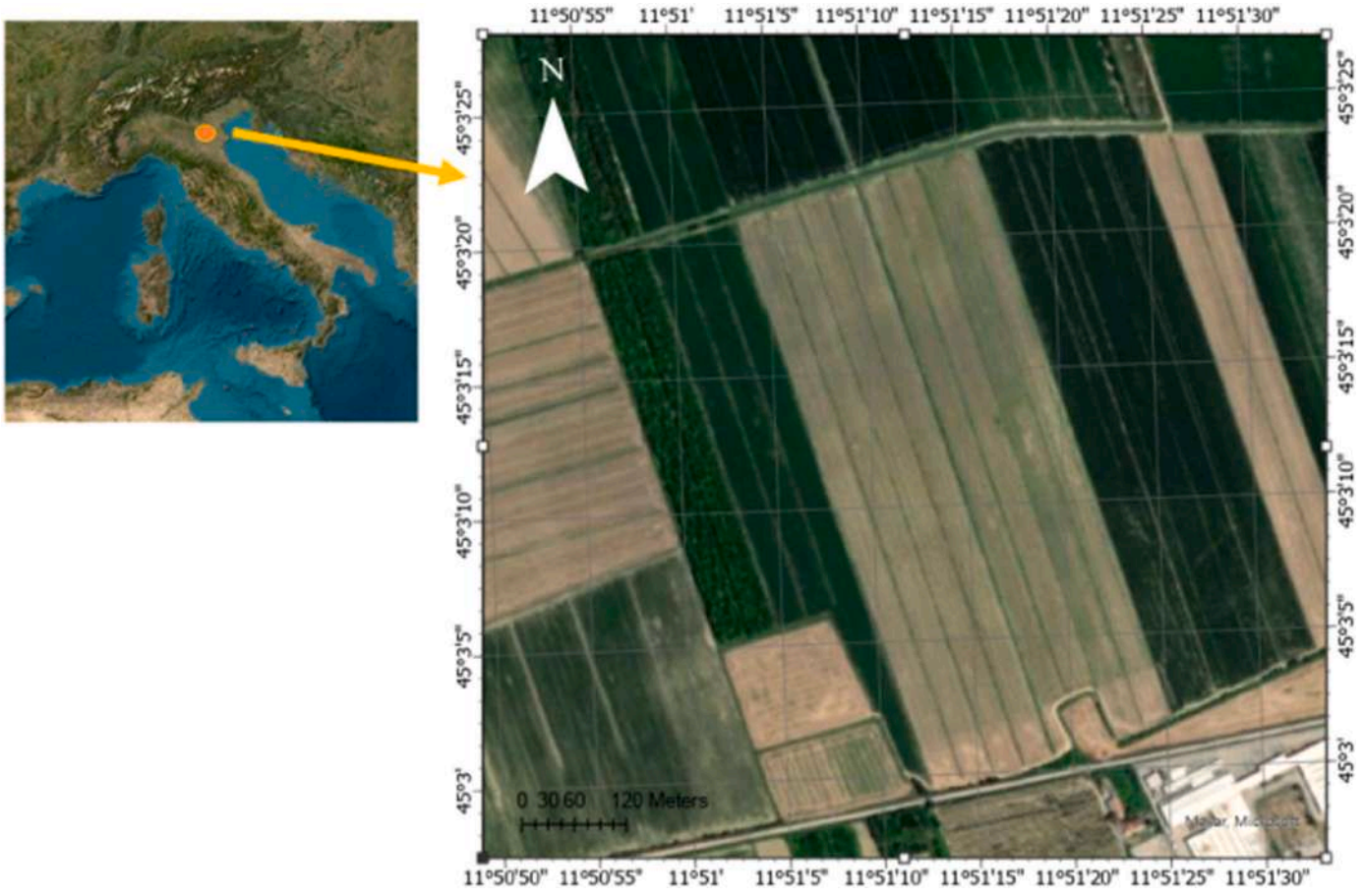

Fig. 1. The experimental site location in the municipality of Ceregnano in Italy.

(Fig. 1), which belongs to the extension service of the Veneto Regional Government (Veneto Agricoltura). The site lies on an alluvial plain, characterized by the presence of paleochannels and in turn high soil spatial variability. Furthermore, depressed areas in the fields originate very shallow water table conditions that can affect crop growth.

The climate is sub-humid, with annual rainfall around 673 mm. In the median year, rainfall is highest in autumn (187 mm) and lowest in winter (129 mm). Reference evapotranspiration (ETo) is 848 mm, with a peak in July (4.8 mm d^{-1}). ETo exceeds rainfall from May to October. The soil is a Endogleyic Cambisols (FAO-UNESCO, 1990) with a silty-loam texture.

Soybean was sowed on May 14th, 2022 and harvested on September 23rd 2022. Tillage operations included a subsoiling at 40 cm depth and seedbed preparation by disk arrow at 20–25 cm depth. No fertilisation was supplied.

Irrigation was provided by a lateral moving machine with sprinklers 284 m long, equipped with a precision irrigation system with a lateral resolution of 34 m. The uniformity of the irrigation system was previously assessed, following the American Society of Agricultural and Biological Engineers (ASABE) standards and resulted in a Hermann and Hein uniformity coefficient of 92%. Water table was maintained fairly shallow in summer in between 60 cm and a maximum around 220 cm with a mean seasonal depth of ca. 150 cm to promote capillary rise which complemented the sprinkler irrigation.

2.1. Ground field measurements

2.1.1. Soil charcterization

The soil was characterized by soil sampling operations which were carried out according to Longo et al. (2020). The apparent electrical conductivity (ECa) measured over the field was used as an ancillary variable for sample selection. Homogeneous zones (Fig. 2) were

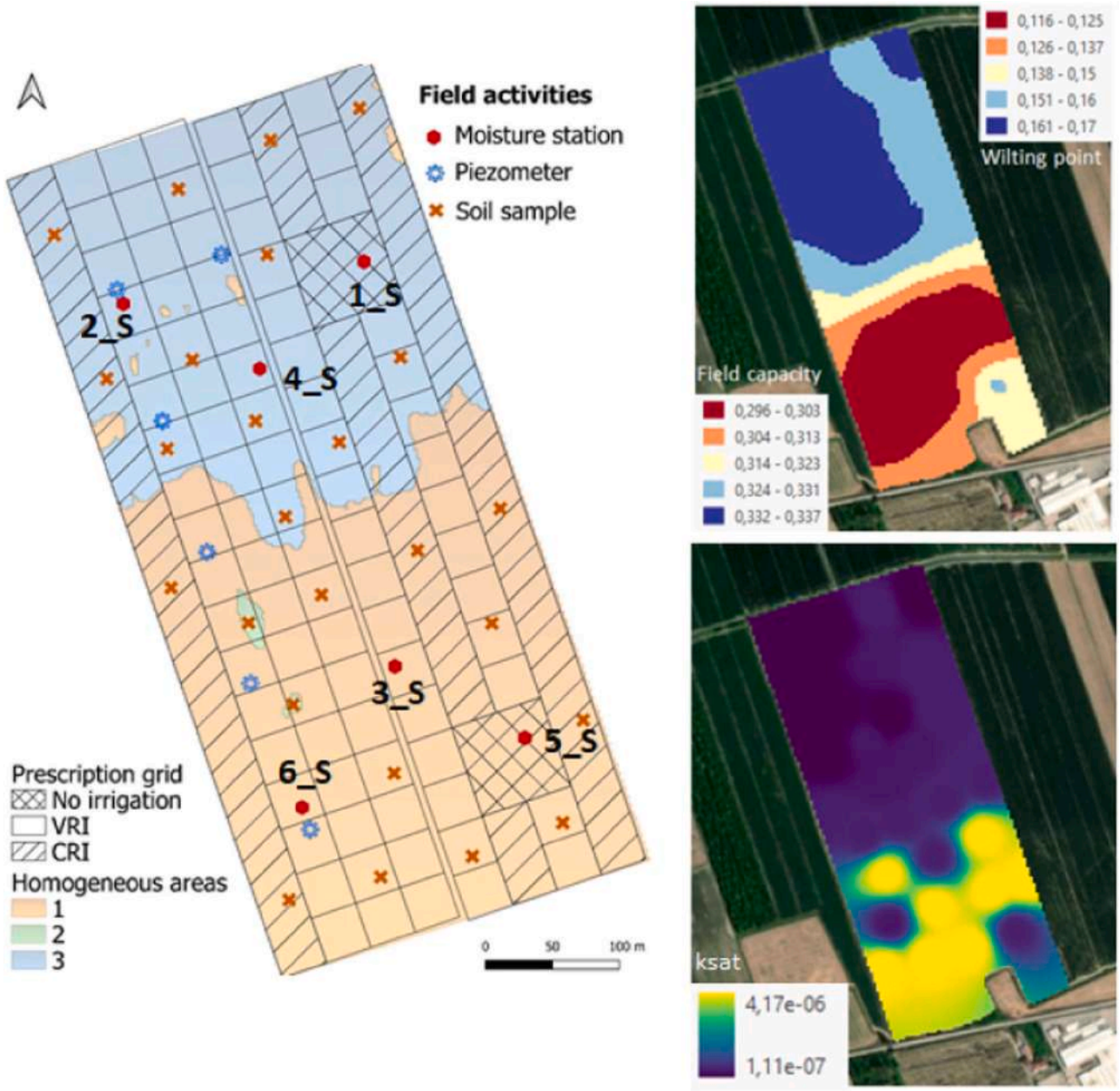

Fig. 2. Left: Homogeneous zones and soil sampling points in Ceregnano site with a) soil moisture stations, b) Piezometers location, c) the irrigation prescription grid: no irrigation, constant irrigation rate CRI, variable irrigation rate (VRI). Right: field capacity (FC) and wilting point (WP) maps (upper), Ks saturated hydraulic conductivity (m s^{-1}) (bottom) obtained from the texture classification.

delineated by ECa maps using a Fuzzy C-means method (Fridgen et al., 2004). An optimal number of samples were then randomly placed within each homogeneous zone (Fig. 2) according to the ECa variability (Longo et al., 2020). In total, 50 disturbed samples (orange cross) were collected at the first 30 cm layer. In addition, at the istallation of 6 moisture stations (red dots), 18 disturbed samples and 18 undisturbed 6-cm cores, were extracted at 10, 30 and 50 cm depths for detailed hydraulic measurements. The disturbed soil samples were analyzed for texture using a laser diffraction granulometer (Bittelli et al., 2022). Texture data were spatially interpolated using the inverse distance weighting method, and a pedotransfer function (Zhang and Schaap, 2017) was then applied to the soil texture maps to estimate soil water retention at 0 kPa, -33 kPa, and -1500 kPa. A RMSE of 5.7 kPa and a R^2 of 0.89 have been found on the accuracy of the pedotransfer function. Saturated hydraulic conductivity (Ks) was measured using a laboratory permeameter (Eijkelkamp, Giesbeek, The Netherlands).

2.1.2. Meteorogolgical data, soil moisture and groundwater level

A weather station (Atmos 41, Meter Group, Inc. USA), was installed near the experimental field to record hourly data of air temperature, precipitation, relative humidity, wind speed and direction, incoming shortwave solar radiation.

Soil moisture sensors were installed in 6 points (Fig. 2) for monitoring the different irrigation treatments. Each station consisted of 3 moisture sensors ('Teros 10' or '5TE' – Meter Group, Inc. USA), wired to a datalogger 'ZL6 basic' (Meter Group, Inc. USA) that recorded data at hourly intervals. Sensors were placed at 10, 30 and 50 cm depth. Prior to field installation soil moisture sensors were previously calibrated in the laboratory to an accuracy of ±2% for 'Teros 10' and ± 3.2% for '5TE'.

Moreover, seven piezometers were placed along a transect at 100-m intervals (Fig. 2) to provide information on a water table gradient in the north-south direction,. An adjunctive piezometer was placed in E-O direction to investigate the effects of the central channel, with a deeper ground water table in the eastern part of the field.

2.1.3. Leaf area index and crop yield map

Leaf area index (LAI) and biomass measurements were collected close to the six monitoring stations, three times during the season (i.e. June 17, July 19 and August 24) (Fig. 2). LAI Accupar LP-80 (Decagon Devices Inc., Pullman, WA, USA) was used for LAI measurements, averaging the values of 3 sub-repetitions. Biomass was collected on 2-m^2 plots, and dried at 65 °C in a forced draft oven for 72 h for dry weight determination. In addition, prior to harvesting, biomass was collected to calculate the harvest index.

Yield data was recorded using a Claas Lexion 780 (Claas Group, Dissen Germany) equipped with a yield monitor and a differential global positioning system. Raw yield data were retrieved by using a digital data transfer system (i.e. TELEMATICS, Class Group, Dissen Germany) cleaned to exclude field-edge effects and harvester manoeuvres using the methodology described in Vega et al., (2019). Yield data were expressed as grain dry matter per hectare (t DM ha^{-1}).

2.2. Satellite data

2.2.1. Land surface temperature retrieval

Split Window technique method was used for LST estimation. It is based on the differential atmospheric absorption of two thermal channels typically located at 10.5–12 μm. General equation of SW algorithm can be found in Sobrino et al., (1996). Test sites monitoring were performed using the Sea and Land Surface Temperature Radiometer (SLSTR) onboard Sentinel 3 which spatial resolution at nadir is 1 km. Particular coefficients of SW for the sensor were taken from Sobrino et al. (2016), where a_0 is equal to 0.0794, a_1 to 1.399, a_2 to 0.1387, a_3 to 50.56, a_4 to -2.730, a_5 to -117.27 and a_6 to 17.88.

The SW equation follows as:

$$T_S = T_i + a_0 - a_1(T_i - T_j) + a_2(T_i - T_j)^2 + (a_3 + a_4 w)(1-\varepsilon) + (a_5 + a_6 w)\Delta\varepsilon \quad (1)$$

where T_S is the LST, T_i and T_j are the at-sensor brightness temperatures at the SW bands i and j (in K), ε is the mean Land Surface Emissivity (LSE), $\varepsilon = 0.5\ (\varepsilon_i + \varepsilon_j)$, Δε is the LSE difference, $\Delta\varepsilon = \varepsilon_i - \varepsilon_j$), w is the total atmospheric water vapor content (in $g{\cdot}cm^{-2}$) and a_0-a_6 are the coefficients.

As the experimental site was too small (on average 25 ha) for the SLSTR pixel, the application of downscaling methods to increase LST spatial resolution was mandatory. The procedure disaggregates coarse thermal data to a finer spatial resolution providing sub-pixel temperatures that meet agricultural requirements for its monitoring. Disaggregation is performed by the use of Nearest Neighbor Temperature Sharpening (NNTS) method which uses the linear relationship between LST and NDVI as well as similar pixel properties and its distance (more weight assigned to the closest similar pixels) to improve the spatial resolution. As Visible and Near InfraRed (VNIR) data is extracted from Sentinel-2 MultiSpectral Instrument (MSI) at a spatial resolution of 10 m, LST subpixels are also provided at this resolution. For more information see Skokovic (2017) and Corbari et al. (2020).

Validation of downscaling procedure was performed comparing Sentinel 3 NNTS images against Landsat 8 (L8) Thermal InfraRed Sensor (TIRS) data. TIRS LST data was directly retrieved from Landsat level 2 products. Comparison was performed when simultaneous pass of Sentinel 3 and Landsat 8 take place although time gap should be take into account for results analysis. Two areas of 200 × 200 m of Ceregnano site representing vegetation and bare soil have been selected for the comparison. As the spatial resolution for both images is not the same, NNTS image was degraded to the spatial resolution of 100 m, which is the TIRS spatial resolution. For both areas and in most of the cases, S3-NNTS and L8-TIRS LST are very similar, showing mean bias and standard deviation below 1.5 °C, and a R^2 of 0.87. When all data are considered, some days present differences above 3 °C, which may be due to time difference (more than 30 min) and presence of clouds in the image.

2.2.2. Vegetation variables retrieval

From NDVI, Fractional Vegetation Cover FVC was estimated, according to Gutman and Ignatov (1998), as:

$$FVC = \frac{NDVI - NDVIs}{NDVIv - NDVIs} \quad (2)$$

where NDVIs and NDVIv are representative NDVI values for bare areas and green vegetation, respectively, and can be retrieved by the use of NDVI histograms. For our case, the maximum and minimum NDVI in a study area are 0.2 and 0.9, respectively, following the algorithm hypotheses of Gutman and Ignatov (1998). For satellite remote sensing data, the Leaf Area Index (LAI) data is retrieved in function of the FVC as (Choudhury, 1987):

$$LAI = \frac{-\ln(1 - FVC)}{k(\theta)} \quad (3)$$

where k(θ) is the light extinction coefficient for a given solar zenith angle. The solar zenith angle (θ) depends on terrain geometry, solar declination, solar elevation angle, latitudinal location and day of the year. The light extinction coefficient is a measure of attenuation of radiation in the canopy. For our test sites, it was calibrated according to ground LAI measurements to 0.5.

Albedo (α) is the fraction of shortwave radiation reflected from the Earth back into space. It is a measure of the reflectivity of the earth's surface. Albedo was calculated as the integration of at-surface reflectance across the shortwave spectrum. Following the relation proposed by Ke et al., (2016) and taking into account that Sentinel 2 and Landsat 8

channels have good agreement and high band value correlation (Barsi et al., 2018), albedo can be estimated as:

$$\alpha_{S2} = 0.130b1 + 0.115b2 + 0.143b3 + 0.180b4 + 0.281b5 + 0.108b6 + 0.042b7 \quad (4)$$

where b is the surface reflectance coefficient for band 1, 2, etc…

Albedo and vegetation variables were retrieved from Sentinel 2 MSI sensor at a spatial resolution of 10 m. The Sentinel 2 L2A product provides the reflectances that are used for NDVI (and then for FCV and LAI) and albedo estimations. Composite images were produced every 15-days, giving more stability to the data.

3. Methodology

The methodology (Fig. 3) that was implemented may be divided into two main steps: 1) step 1 refers to the calibration and validation of the hydrological model, and 2) step 2 refers to the use of the model for the estimation of the irrigation prescription maps. These maps have been then uploaded in the irrigation machine system for providing irrigation to the field during the crop season.

3.1. The FEST-EWB-SAFY model

The crop-energy-water balance FEST-EWB-SAFY model (Corbari et al., 2022) couples the distributed energy-water balance FEST-EWB (Corbari et al., 2011), which allows computing continuously in time and distributed in space both soil moisture and effective evapotranspiration fluxes, and the SAFY (Duchemin et al., 2008), simple model for yield prediction and plant development. The workflow is shown in Fig. 3.

More specifically, the FEST-EWB model is based on the system of energy-water balances equations which are written in terms of the LST, as the land surface temperature that allows closing the energy balance equation, so that this model internal variable can be directly compared with remotely sensed LST. The SAFY model (Simple Algorithm for Yield Estimates) is a parsimonious agronomical model that simulates the Green Area Index (GAI) and Dry Aboveground Mass (DAM) at a daily time step (Duchemin et al., 2008), combining the Monteith's light-use efficiency theory with a leaf partitioning function.

The system of the soil water balance for the superficial and deeper layers and energy balance together with the LAI and biomass evolution is calculated for each single pixel, as:

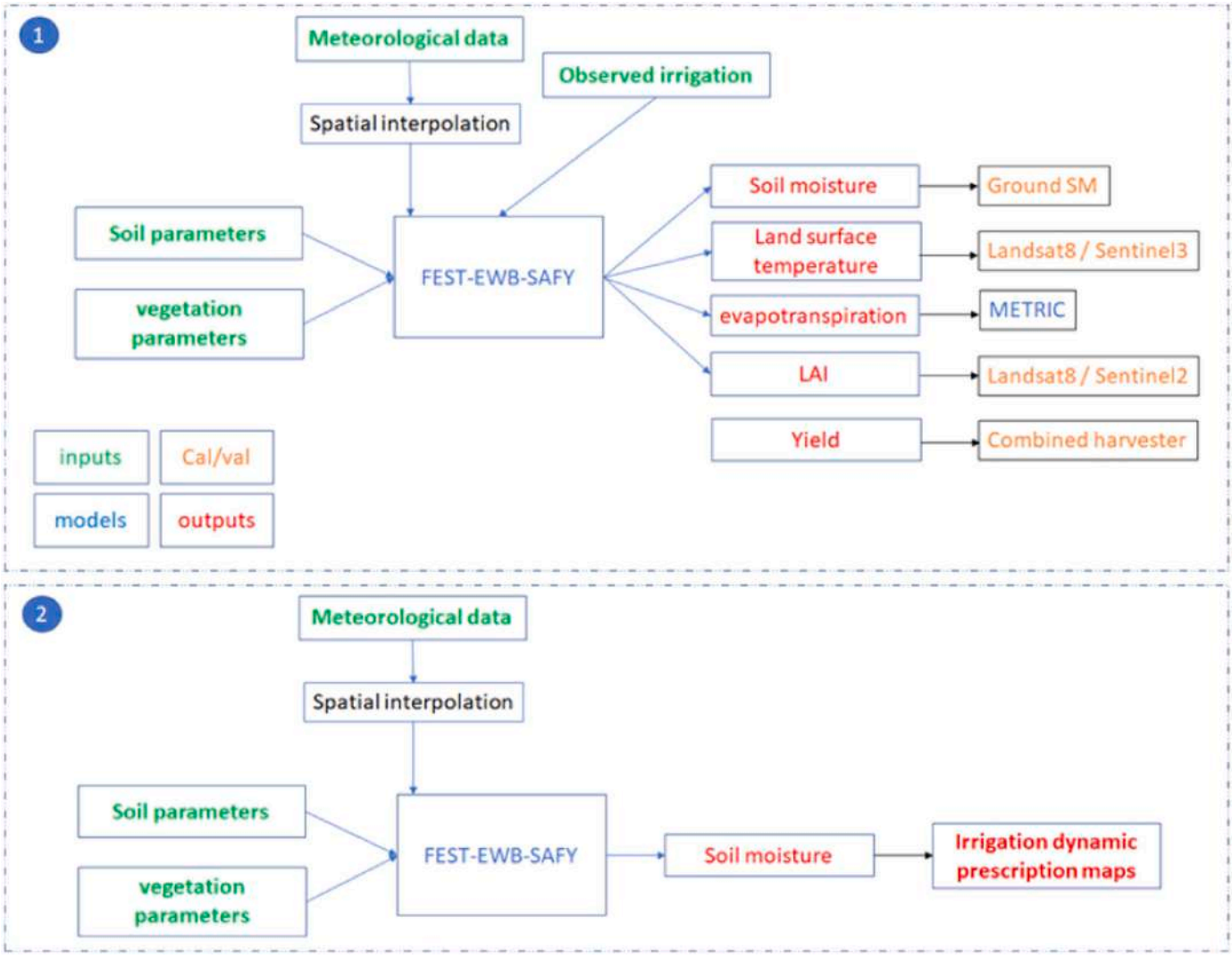

Fig. 3. Workflow of the methodology implemented.

$$\begin{cases} \frac{\partial SM_{(1)}}{\partial t} \bullet \Delta z_1 = P + I + C_{(1)} - Pe_{(1)} - \beta \quad ET \\ \frac{\partial SM_{(2)}}{\partial t} \bullet \Delta z_2 = Pe_{(1)} + C_{(2)} - C_{(1)} - Pe_{(2)} - \delta \quad ET \\ Rn - G - H - LE = 0 \\ \Delta DAM = APAR * ELUE * f(Ta) * K_{stress} \end{cases} \quad (5)$$

where $SM_{(1)}$ and $SM_{(2)}$ refer to the soil moisture of the superficial and deep layers, respectively (-), P to the precipitation rate (mm h^{-1}), I to irrigation (mm h^{-1}), Pe_1 to the drainage flux from the shallow layer to the deeper one (mm h^{-1}), while Pe_2 from the deeper one (mm h^{-1}), ET to the effective evapotranspiration (mm h^{-1}), Δz_1 is the superficial soil depth (m) and Δz_2 the deep soil depth (m), C_1 is the capillary rise between the two layers (mm h^{-1}) and C_2 between the deep layer and the groundwater table (mm h^{-1}), Rn (W m^{-2}) is the net radiation, G (W m^{-2}) is the soil heat flux, H (W m^{-2}) is the sensible heat flux, while LE (W m^{-2}) is the latent heat flux. The total evapotranspiration from the soil layers is partitioned into the shallow-layer (ET_1) and the deep-layer (ET_2) components.

The DAM production is a function of the effective light-use efficiency (ELUE), the daily temperature (T_a) and the daily photosynthetically active radiation absorbed by the canopy (APAR). Its time evolution could be impacted by air temperature (f(Ta)) or water stress (K_{stress}) based on soil moisture.

A complete description of the model is in Corbari et al. (2022).

FEST-EWB model has been demonstrated to be able to simulate ET and SM at local scale against eddy covariance stations measurements (Paciolla et al., 2021) as well as at Irrigation Consortium scale in comparison to satellite land surface temperature (LST) data considering also irrigation water management (Corbari and Mancini, 2023).

Thus, the FEST-EWB-SAFY model was implemented at Ceregnano site for the year 2022 from May to the end of August at 1-hour temporal resolution and at 10 m spatial resolution.

The main input parameters to the model are: (1) meteorological forcings: air temperature and relative humidity, incoming shortwave radiation, wind speed and rainfall; (2) maps of soil hydraulic parameters (as hydraulic conductivity, FC, WP, …); (3) vegetation parameters (effective light-use efficiency, crop resistance to ET, …); (4) maps of albedo from Sentinel 2; (5) groundwater level; (6) irrigation volume. The full list of model parameters is listed in Corbari et al., (2011), (2022).

The model was calibrated and validated by comparison with different ground and satellite data, to be able to verify multiple component of the soil-plant-atmosphere water cycle. Firstly, the water-energy budget dependent parameters have been calibrated pixel by pixel looking for the minimization of the Root Mean Square Error (RMSE) between the simulated land surface temperature and the observed satellite LST in each single pixel, based on the procedure developed by Corbari and Mancini (2014), where each single pixel parameter is tuned independently from the other pixels. Similarly, the crop growth parameters have been calibrated pixel wise minimizing the difference between modeled and remotely-observed LAI. The model has then been validated against ground measurements of soil moisture at different depth and combined harvester crop yield map.

The FEST-EWB-SAFY is thus not using satellite data of LST and LAI as input (besides albedo which is updated when available), as most of the satellite based models do, but they are used only for calibration purposes. So the model is independent from the revisit time of satellite or the presence of clouds in the image.

3.2. The METRIC model

METRIC (Mapping Evapotranspiration with Internalized Calibration) is a satellite-based image-processing tool for calculating ET and Kc stress coefficient (Allen et al., 2007). ET is calculated as a residual term of the energy balance at the Earth's surface as follows:

$$LE = Rn - G - H \quad (6)$$

Where, LE (W m^{-2}) is the latent energy, Rn (W m^{-2}) is the net radiation, G (W m^{-2}) the sensible heat flux, and H (W m^{-2}) is the sensible heat flux convected to the air.

When using satellite imagery, sensed surface radiances are converted into surface properties such as albedo, vegetation indices, surface emissivity and surface temperature. These products are then used to estimate the various components of energy balance. METRIC also needs weather data, such as air temperature, relative humidity, wind speed, rain and solar radiation. Ground based information is also crucial to internally calibrate the model, calculating reference ET, reducing the computational biases resulting from remote sensing operations.

As part of the calibration process, identification of a "cold" and "hot" pixel is required for the H computation. These pixels represent the largest and lowest ET (i.e., bare soil), respectively.

METRIC is a tool developed and widely used with Landsat and MODIS imagery, whose spatial and temporal resolutions are not fully suitable for precision agriculture applications. The high spatial (10 m) resolution LST maps created by the sharpening techniques allowed to adapt METRIC to the small-size Italian fields. In addition,the high temporal resolution (<5 days) also allowed to improve model simulations.

3.3. Irrigation treatments

Irrigation test was conducted in July and August 2022, comparing VRI treatment driven by FEST-EWB-SAFY with a uniform treatment (CRI). The experimental design involved incomplete randomized blocks with five replicates for VRI and three replicates for CRI, each one consisting in 2.2-ha plot.

Prescription maps were generated during the season based on crop water requirements, calculated on 30x30m pixel resolution in VRI. The prescription grid is shown in Fig. 2, highlighting the VRI areas, as well as the area where a uniform irrigation has been applied and two control areas where no irrigation was performed. Irrigation volumes were determined as a difference between field capacity and soil content in the first 50-cm soil profile where approximately 80% of the root biomass was concentrated (Piccoli et al., 2021). Irrigation was scheduled to keep the soil moisture content above the lower limit of the readily available water content, estimated to be equal to 50% of the available water content (Allen et al., 1998). Uniform irrigation volumes were calculated according to the business-as-usual method based on soil water content measured by the moisture sensors. A system efficiency of 95% has been considered.

Irrigation performances were evaluated in terms of crop yield, irrigation volumes and the irrigation water productivity (WP). This last is computed as:

$$WP = \frac{crop\ yield(kg)}{irrigation\ volume(m^3)} \quad (7)$$

ANOVA was used to evaluate the effect of irrigation treatments on irrigation volumes, yield and agronomic efficiency. For all the analyses, $p < 0.05$ indicated a significant difference between means.

4. Results

4.1. Model calibration and validation

4.1.1. The water-energy balance component

The FEST-EWB-SAFY model produced as outputs hourly land surface temperature maps, which were used for calibrating the model in its internal variable processes linked to the water-energy balance. A total mean bias of 1.4 °C and an absolute difference of 1.9 °C were found over the five available LANDSAT images, with a 0.97 coefficient of the linear

regression with R^2 of 0.74, showing the consistency of the estimates and the ability of the model in reproducing the spatial and temporal variability of observed LST. The model LST estimates were also compared with the downscaled Sentinel3 LST images over a total of 89 dates, resulting in a mean bias of 1.1 °C and an absolute one of 2.7 °C. The linear regression was also computed obtaining a slope of 0.92 and R^2 of 0.70. In Fig. 4, the mean and absolute differences maps between the modelled LST and the acquired from both LANDSAT and Sentinel3-NNTS are shown. Thanks to the high spatial resolution of both this last and the model images, detailed features are visible showing higher absolute errors and a model underestimation in the southern part. This might be due to differences in crop evolution where the area is characterized by a lower LAI in respect to the northern part of the field as well as different soil characthersitcs with more sandy soils.

The model was validated in its soil water-energy part by comparison with the soil moisture content measured by the six stations at 10 cm and 50 cm (Fig. 5). A mean bias of -0.01 and -0.03 are obtained for the two increasing depth with a RMSE of 0.06 and 0.03, respectively (Table 1). Table 1 shows also the R^2 and the slope of the linear regression (m). The model exhibits some difficulties in the representation of the deeper SM for stations S1, S3, S4 and S6 where the groundwater rise plays a predominant role at the end of the season.

No water stress was observed during the growing season. Soil moisture reached minimum values between June and August, returning to field capacity after heavy rainfalls at the end of August. In general, soil moisture never fell below the lower limit of the readily available water, set equal to 50% of the available water capacity, however drier conditions were observed in the southern zone of the field. A clear difference is observable among stations S5 and S6 and the others, due to the different soil type of the area with lower sand contents than the rest of the field. The deepest SM is sustained through the season mainly by the groundwater rise. The superficial soil moisture values are instead clearly

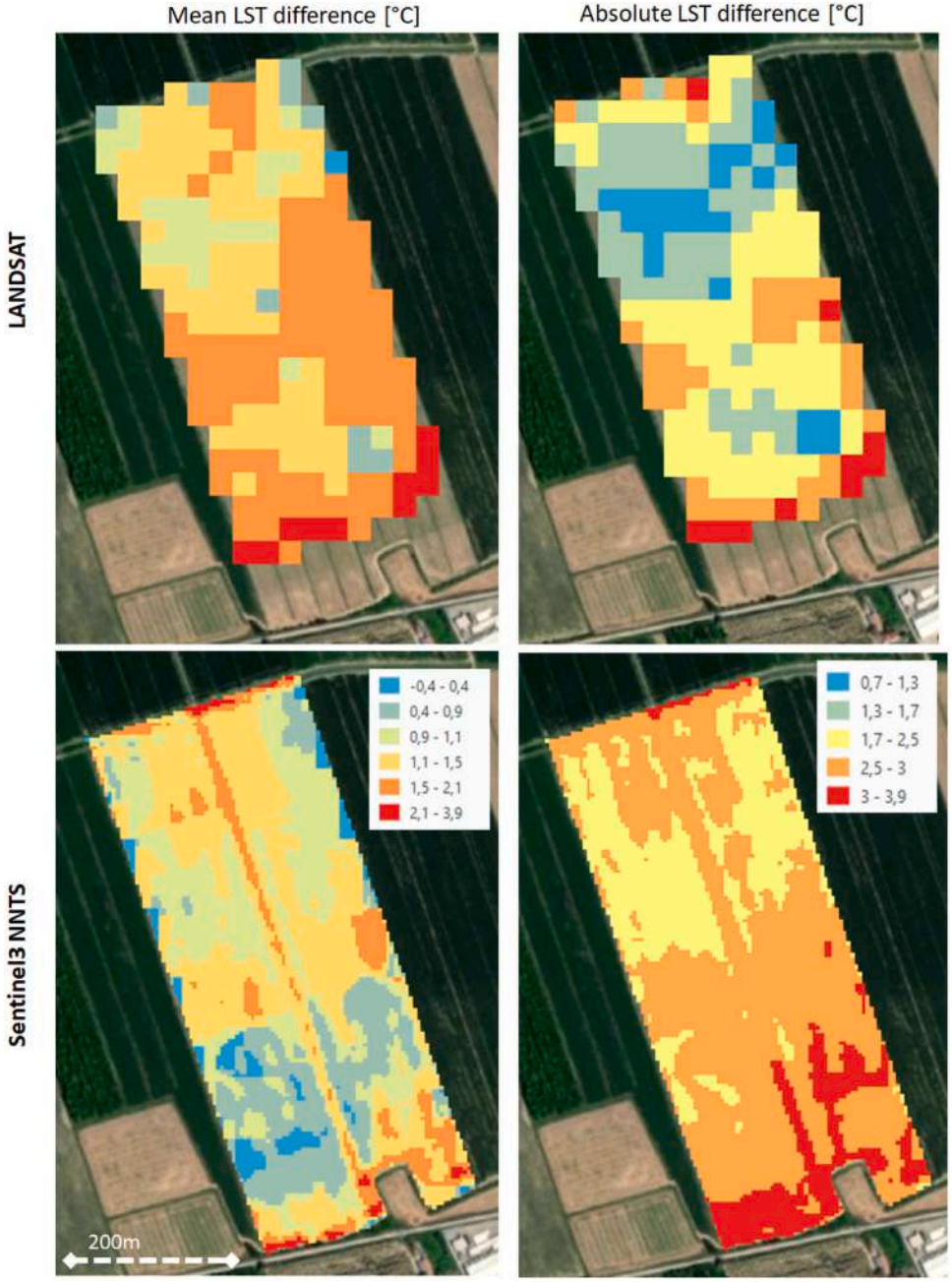

Fig. 4. The mean and absolute differences maps between the modelled LST and the acquired images from LANDSAT (upper) and Sentinel3-NNTS (bottom).

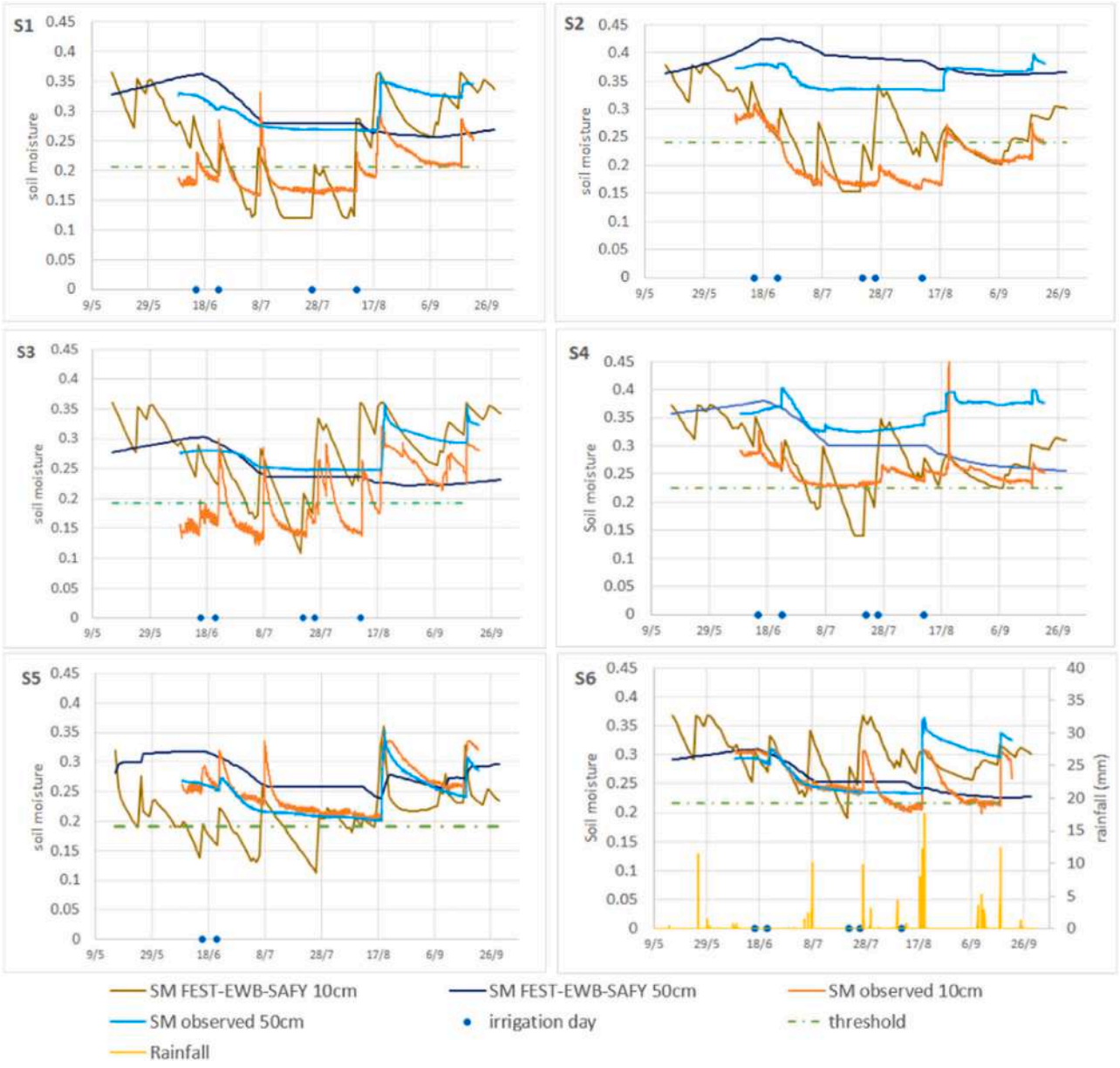

Fig. 5. Soil moisture dynamic at the 6 ground stations at 10 cm and 50 cm from ground observation and FEST-EWB-SAFY model at Ceregnano site.

Table 1
Soil moisture errors at the 6 ground stations between ground observations and FEST-EWB-SAFY model.

	sm 10 cm			sm 50 cm		
	BIAS	RMSE	m (R^2)	BIAS	RMSE	m (R^2)
station S1	0.07	0.08	0.82 (0.75)	-0.03	0.04	1.03 (0.55)
station S2	-0.05	0.07	0.83 (0.67)	-0.04	0.05	0.87 (0.53)
station S3	-0.05	0.08	0.95 (0.78)	0	0.02	1.01 (0.49)
station S4	-0.02	0.06	0.94 (0.78)	-0.1	0.03	1.01 (0.49)
station S5	-0.01	0.04	1.1 (0.55)	-0.03	0.04	0.87 (0.56)
station S6	0	0.04	0.88 (0.68)	-0.02	0.03	1.01 (0.58)

affected by the precipitation events, as well as the "planned" irrigations. However, it is interesting to note that sensors at 10 cm are not seeing the low intensity events due to the presence of dense vegetation which intercepts much of the water.

Finally, as a mean of validation, the evapotranspiration estimates from the crop-water-energy balance FEST-EWB-SAFY were compared with the ET maps computed from the residual energy balance model METRIC. The main models difference relates to the use of the satellite LST, which is used as input variable in the METRIC model while the FEST-EWB model uses it as calibration variable. Thus, FEST-EWB-SAFY model is able to compute ET values continuously in time (every hour/day), while the METRIC model only at satellite overpasses. In Fig. 6 the comparison between the instantaneous estimates of evapotranspiration from the two models is showed for two available dates of LST cloud-free images from LANDSAT 9: 16 May, 3 July and 3 August 2022, reporting a good spatial agreement. A mean bias of 0.14 mm day^{-1} has been observed. The linear regression was also computed obtaining a slope of 0.97 and R^2 of 0.8.

4.1.2. *The crop growth component*

The calibration of the crop growth parameters followed as well the pixel-by-pixel procedure accounting for the differences between the simulated and the satellite observed LAI maps in each single pixel. Thus, the model parameters were modified in each pixel independently one from the other. In Fig. 7, as example, the LANDSAT satellite and simulate

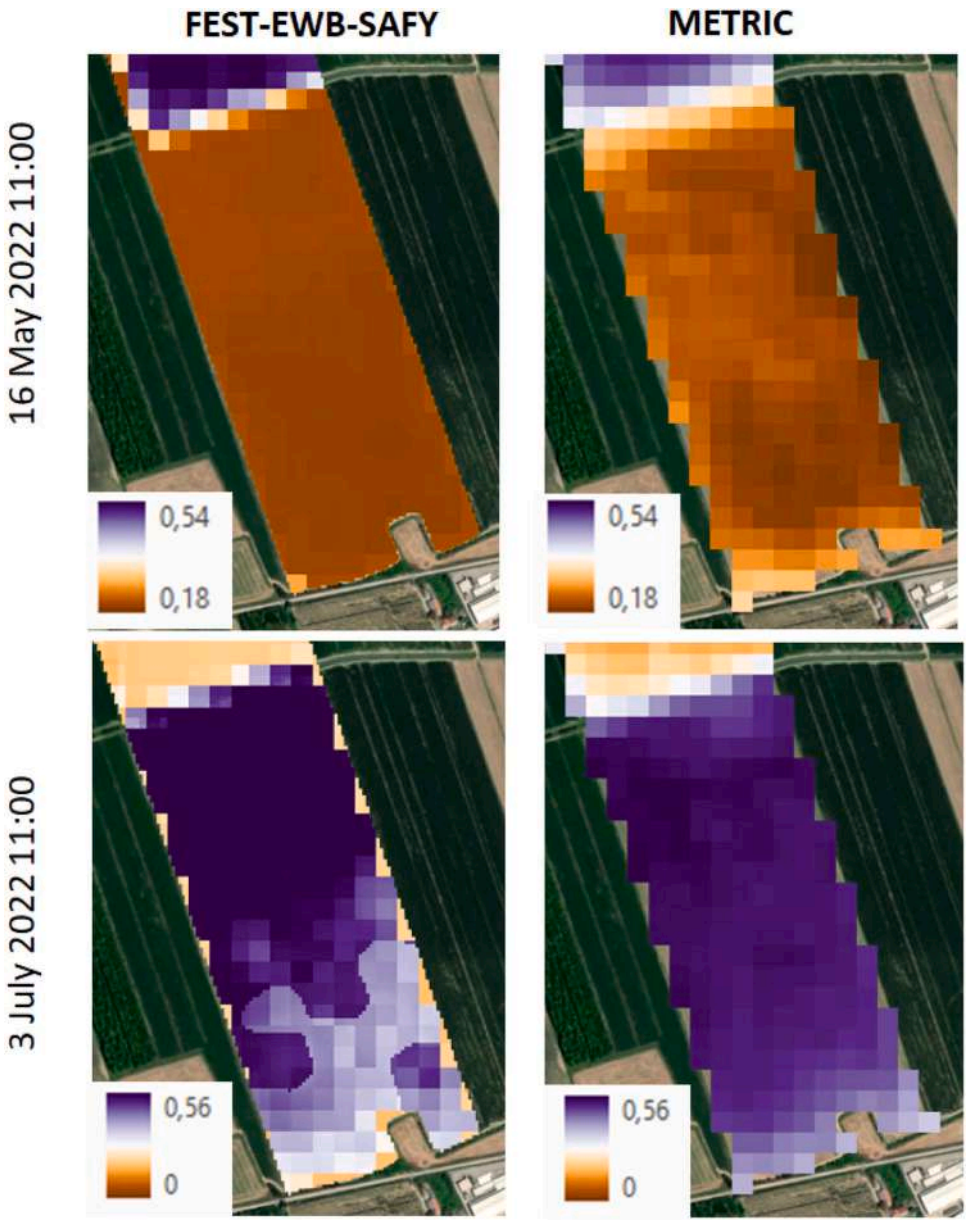

Fig. 6. Instantaneous ET maps from LANDSAT and from FEST-EWB-SAFY model at Ceregnano site for 16 May and 3 July 2022 at 11:00.

maps of the 4th August 2022 are shown, highlighting the field spatial variability of the satellite image as well as of the modeled map after the calibration, with the northern part of the field characterized by more developed vegetation than the southern part. In Fig. 7, the leaf area index temporal dynamic is also consided for the monitoring stations allowing to follow the whole crop season from the crop emergence to the fully developed stage till the harvest. It is also interesting to note the high intra-field variability between station 1 (similarly to 2, 3 and 4) being charactherized by higher LAI values than station 6 (similarly to 5). This is true for both the model estimates and the satellite data; while the model allows to close the temporal gap of satellite data aquisition providing daily time in continuous estimates.

For evaluating the accuracy of the calibration process, all the available images were compared at the LANDSAT spatial resolution and the mean and absolute differences maps was computed (Fig. 8), showing area average values of -0.15 and 0.39, respectively. Lower errors were obtained in the shouthern part of the field.

By comparison of the modeled and observed yield from the combined harvester, a map of total yield was calibrated for the FEST-EWB-SAFY model (Fig. 9), reaching a mean error of −120 kg ha^{-1} with a standard deviation of 350, and an absolute mean difference of 220 kg/ha. Crop yield was significantly affected by groundwater table depth, which varied from −99 cm in the northern stations to −156 cm in the middle of the field to -220 in the southern stations. A shallow aquifer in the northern area led to average crop yield 5 t ha^{-1} compared to the southern area with crop yields of 3.5 tha^{-1}, on average.

To better understand the influcence of soil properties, crop water use and crop growth on yield spatial variations, a 3D correlation was built between yield, cumulated ET over the season and the maximum LAI (Fig. 10). An almost linear correlation, as expected, is observable between yield and ET, while not always higher yields correspond to higher LAI values. This might be due to the considerable difference in spatial resolution between the combine harvester yield map (5 m) and the LANDSAT LAI data (30 m) which could correspond to a loss of information with averaging high with low values, as well as to the limit of satellite images to correctly estimate high values of LAI after a certain high threshold leading to LAI underestimation. Similarly, high differences are found according to the variability of soil type, being the

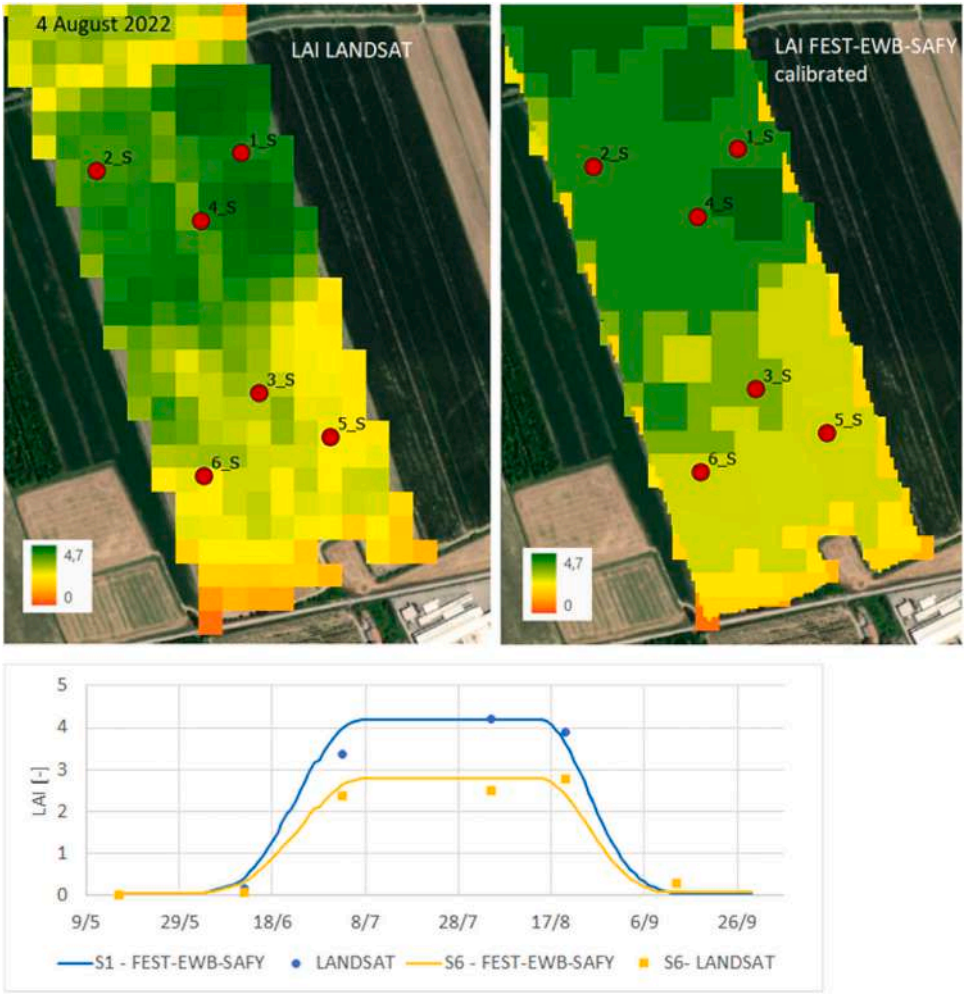

Fig. 7. Comparison of LAI map of 4 August 2022 measured from satellite and modeled from the FEST-EWB-SAFY model before and after calibration, (bottom) comparison of modeled and observed LAI dynamic at stations pixels.

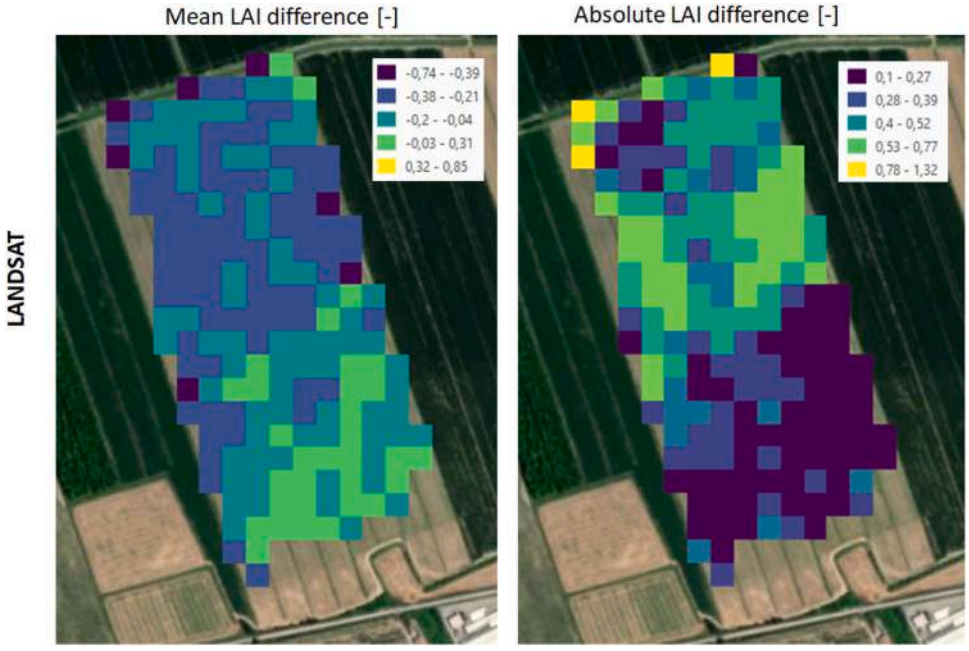

Fig. 8. The mean and absolute differences maps between the modelled and the LANDSAT LAI at the satellite spatial resolution.

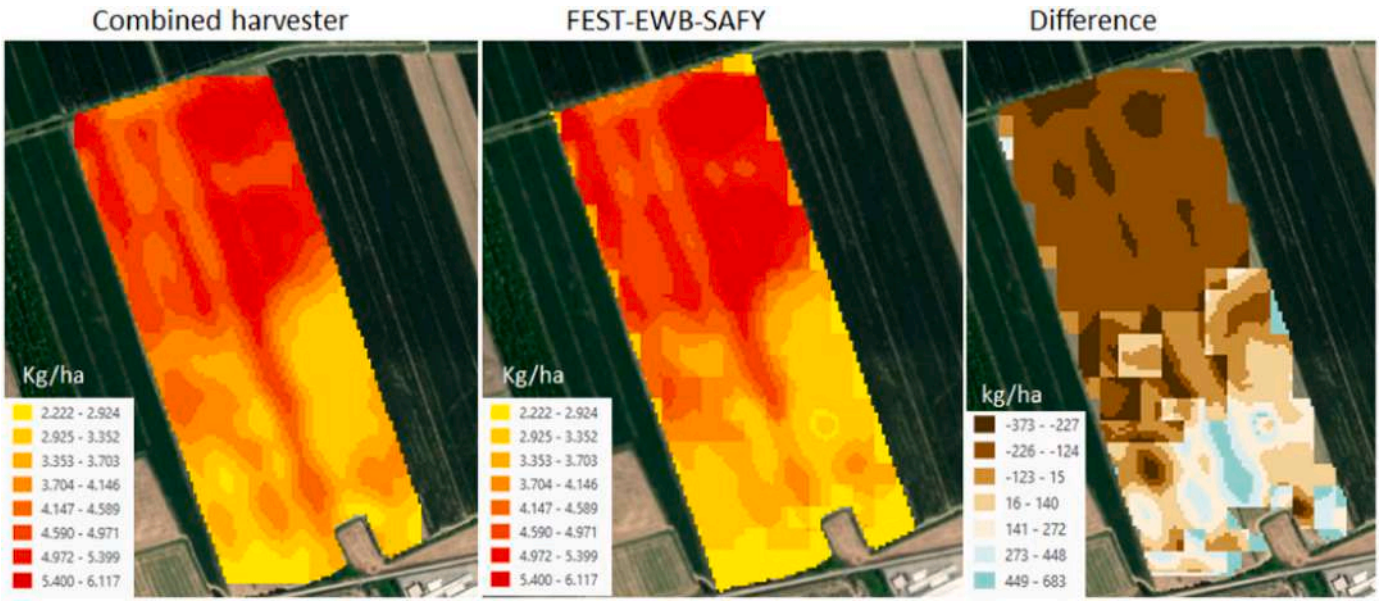

Fig. 9. Comparison of modeled crop yield and observed yield from the combined harvester.

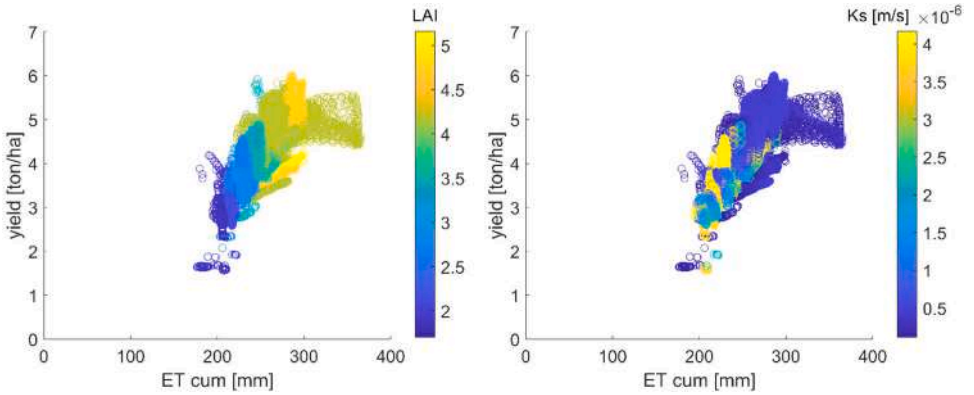

Fig. 10. 3D correlation between crop yield and cumulated ET over the season colored by the maximum LAI for 2022 (left) and the saturated hydraulic conductivity (right).

northern part of the field chartactherized by more silty soils while in the southern part more sandy soils are present. This is inversely linearly correlated with crop yield and LAI with the lower permeability zones which reported higher crop yields.

4.2. Irrigation prescription maps

Irrigation operations began in June with two uniform applications of 30 mm on June 15, 2022, and 50 mm on June 22, 2022, applied over the study site. VRI was conducted during July and August following soil characterisation and model implementation. Three VRI irrigation events took place on 23/7/2022, 27/7/2022, 11/8/2022, using the calibrated soil moisture maps estimated from FEST-EWB-SAFY model to create the irrigation prescription maps. To note, two areas encompassing soil moisture stations 1 and 5 were intentionally kept without irrigation for water stress control. Data collected in the two areas were not analyzed.

In Fig. 11, as example, the soil moisture distribution at 50 cm is shown for the on 10 August 2022 as simulated by the FEST-EWB-SAFY model., whene critical soil moisture values for crops started to appear. This information was thus used to suggest an irrigation prescription map. Irrigation values showed a large variability ranging from 35 mm to 21 mm, with the highest volumes applied in the uniform treatment.

The maps of the total irrigation volumes, crop yield and the water use efficiency (Fig. 12) allow to clearly identify a spatial variability within the field, with a decreasing gradient of the variables from north to south. Although the short period of comparison, VRI allowed to reduce the irrigation volume from 155 mm to 140.3 mm ($p<0.05$), without a significant contraction of crop yield, that was on average 3.64 t ha^{-1}. Accordingly, WP increased from 2.3 kg m^{-3} to 2.6 kg m^{-3}. Similar estimates of WP are obtained when using either the crop yield map from the combined harvester machine or the FEST-EWB-SAFY model. These maps were then averaged within the identified areas subjected to the different irrigation regimes: the constant rate irrigation and the variable rate irrigation. Although VRI was applied only in 3 out 5 irrigation events, the results highlighted the positive aspects of the VRI, which allowed to slightly reduce irrigation volumes and increase the water use efficiency.

5. Discussion

This study investigated quantitatively how a new model-based and remote sensing method can help to overcome traditional irrigation system. The crop-energy-water balance FEST-EWB-SAFY allowed the creation of irrigation dynamic prescription maps, following the variations of the daily water requirement resulting from ET processes, soil properties and field management.

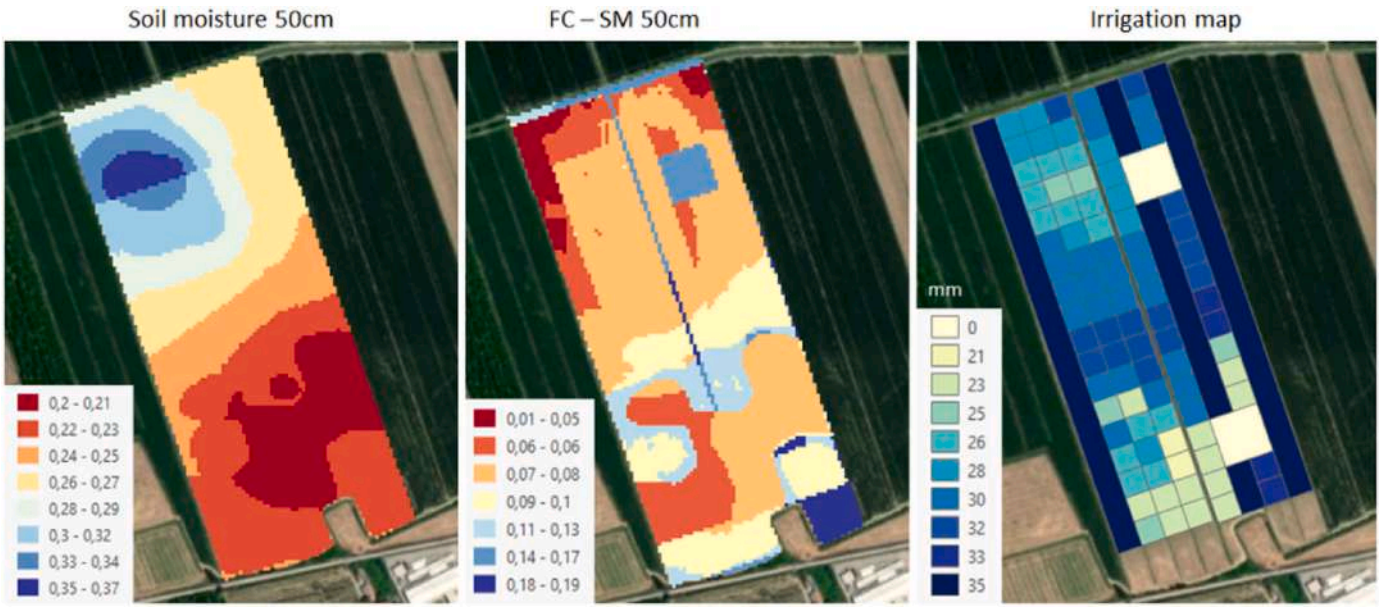

Fig. 11. Soil moisture map at 50 cm, the difference between field capacity and soil moisture and the irrigation prescription map from FEST-EWB-SAFY model for 10 August 2022.

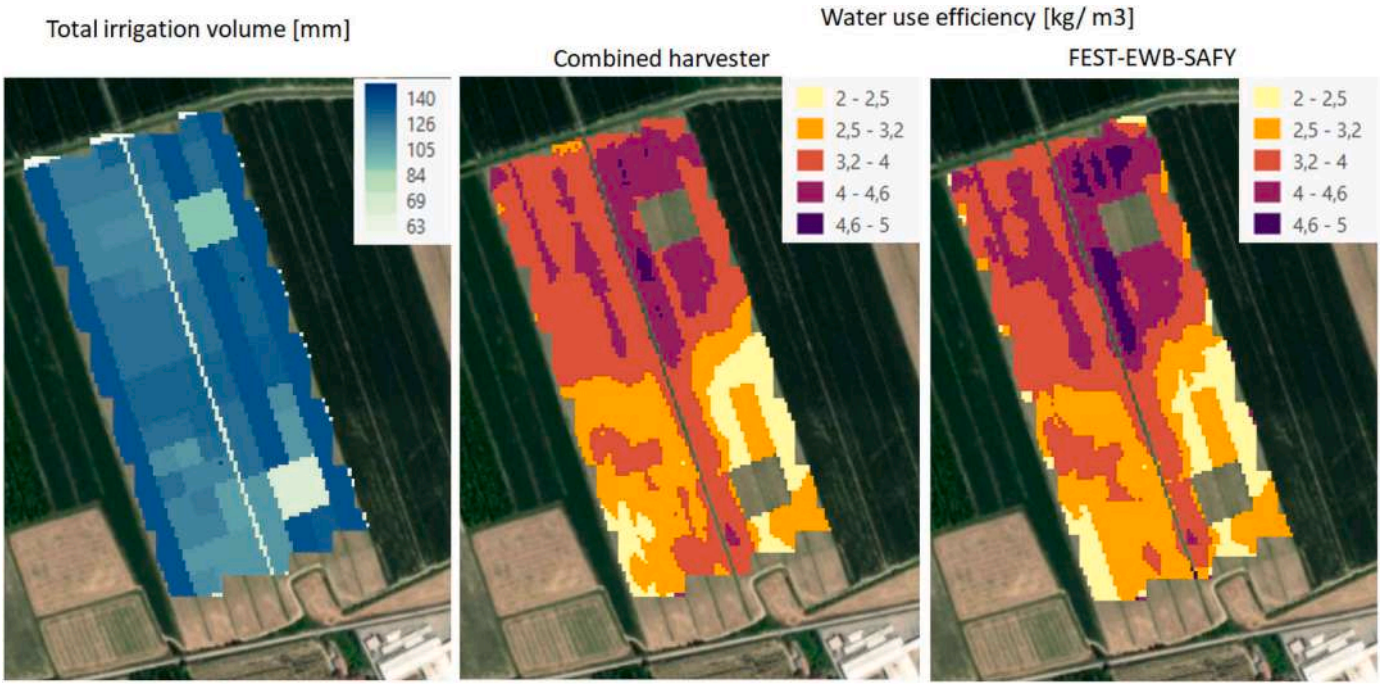

Fig. 12. Maps of total irrigation volumes and of the water use efficiency from the combined harvester and the FEST-EWB-SAFY model.

5.1. Comparison with previous studies

By comparing VRI with traditional irrigation systems, the results of this work showed a positive effect on the water use efficiency due to a consistent water saving without causing negative consequences in terms of crop yield. The obtained results are of particular interest because time variable pixel based maps have been produced, while previous applications are mostly based on irrigation management zones (O'Shaughnessy et al., 2016).

According to the review from O'Shaughnessy et al. (2019), the VRI technology has been used for about 20 years to optimize the irrigation efficiency avoiding under- and overwatering, accounting for variations is soil type, salinity, topography, or non homogeneous planting. However, the irrigation management zones created from these factors are fixed along the crop season and do not account for the changes in crop water requirements and crop water stress conditions (Falkenberg et al., 2007). Some examples of accounting the time variabity of irirgation water requirements are available based on ground measurements of soil moisture or leaf water content (Gobbo et al., 2019; Vellidis et al., 2013). The main strenght of the results obtained from this paper is the possibility of defining dynamic prescription maps which account for spatial and temporal variability of all the mentioned factors affecting the irrigation water needs, with a resolution of 10 m daily. No other examples have been found by the authors in literature.

In general the obtained results on the adavantage of using a VRI system is in accordance with previous studies, as the results obtained by Sui and Yan (2017) who found a water saving of 25% and a small yield increase (2.8%) if using a VRI system in comparison to a CRI one. Similary, also Zhao et al. (2017) and Li et al. (2018) found a higher WP for winter wheat and maize if a VRI system is used.

This confirmed that the model-based dynamic prescription maps could be used to optimize variable irrigation in highly spatio-temporal dynamic cropping systems. In particular, the FEST-EWB-SAFY approach allowed improving the traditional ET based estimates of remote-sensing residual models (e.g TSEB, SEBS, METRIC among others) or approaches based on FAO crop coefficient. In fact, the FEST-EWB-SAFY scheme allowed to: 1) overcome the issue of satellite data availability (limited by clouds and satellite revisit time), because unlike most models, which require LST as an input, FEST-EWB computes LST as an internal variable and has physically-based, non-residual formulations for the components of the energy balance (Bastiaanssen et al., 1998; Su, 2002; Norman et al., 1995); 2) to compute the soil moisture dynamic continuously in time and distributed in space for different soil layers. One of the strengths of the FEST-EWB-SAFY model is that satellite data of LST and LAI are used for model calibration, and that the model could be validated against independent variables as soil moisture and crop yield, as demonstrated by Corbari and Mancini (2014). Similary, Duethmann et al. (2024) showed that a calibration based on land surface temperature improves the spatial pattern of evapotranspiration estimates. Moreover, the developed procedure could also differ from the crop coefficient based methods which relieson keeping the ET close to potential (D'Urso, 2010; Vuolo et al., 2015; Calera Belmonte et al., 2017).

5.2. Limitations of the modeling approach and possible improvements

The accuracy of the estimates of the FEST-EWB-SAFY could be improved considering the different processes representation as well as the quality of the data used for calibration and validation.

Part of the uncertainty could be attributed to the satellite data accuracy and their spatial resolutions, as spatial and spectral accuracy can cause data inconsistencies between the Sentinel and Landsat LAI estimates (Jin et al., 2019). As well, satellite LST data might be also affected by errors, mainly due to the retrieval algorithm, the definition of satellite LST over heterogeneous area, the angle of view of the sensor and the surface emissivity (Sobrino et al., 2015; Kustas et al., 2004).

The model has been validated against local soil moisture values measured by six ground sensors which are not covering the entire field area (although they have been installed to cover the main classes of soil type and water table levels), limiting their capacity in correctly reproducing the spatial distribution of soil moisture.

Another source of uncertainty might be linked to the hypotheses of the crop growth model, SAFY, which is based on a simple algorithm with few parameters (Duchemin et al., 2008), specifically designed for satellite based applications over large areas. This might lead to higher uncertainties in respect to more complex crop models which rely on a larger number of paramters (Dyke et al., 1986; Brisson et al., 2003).

To reduce model uncertainty, data assimilation techniques could be implemented to constrain one or multiple variables, as LST, LAI or SM to indirectly consider the impacts of, for example, variations in soil moisture and crop stress. Several studies assimilated satellite LAI or vegetation fraction to improve crop prodcution (Wang et al., (2013); Chen et al., (2018); or other studies used satellite SM for improving ET estimates (Zhang et al., 2020; Lu et al., 2021).

6. Conclusions

The FEST-EWB-SAFY model which couples the distributed energy-water balance FEST-EWB, which allows computing continuously in time and distributed in space both soil moisture and evapotranspiration fluxes, and the crop growth simple model SAFY, was applied in a 17.6 ha field cultivated with soybean in 2022 at Ceregnano, to generate dynamic irrigation prescription maps. The model was pixelwise calibrated with remotely sensed land surface temperature (RMSE 1.3 °C) and leaf area index (RMSE 0.45) as well as local measured soil moisture at 10 cm and 50 cm depth (RMSE 0.04). The model estimates of crop yield correlated also well with the combined harvester measurements (an absolute mean difference of 220 kg/ha).

FEST-EWB-SAFY allowed the creation of three dynamic prescription maps (over a total of 5 irrigations). Comparing VRI with traditional irrigation systems, the results of this work showed a positive effect on the water use efficiency due to a consistent water saving without causing negative consequences in terms of crop yield.

CRediT authorship contribution statement

Francesco Morari: Writing – review & editing, Writing – original draft, Supervision, Methodology, Funding acquisition, Formal analysis, Conceptualization. **Josè Sobrino:** Writing – original draft, Resources, Methodology. **Drazen Skokovic:** Writing – original draft, Formal analysis, Data curation. **Jacopo Furlanetto:** Formal analysis, Data curation. **Lorenzo Furlan:** Data curation, Conceptualization. **Davide Gabrieli:** Investigation, Formal analysis, Data curation. **Chiara Corbari:** Writing – review & editing, Writing – original draft, Methodology, Investigation, Funding acquisition, Formal analysis, Conceptualization.

Declaration of Competing Interest

The authors declare that they have no known competing financial interests or personal relationships that could have appeared to influence the work reported in this paper.

Data availability

Data will be made available on request.

Acknowledgement

This research was funded by the European Space Agency withing the project "HYPER-CROP – hyper-resolution crop yield estimates and extreme events crops shocks monitoring by integrating multiple satellite data and monitoring" https://eo4society.esa.int/projects/hyper-crop/.

References

Alexandratos et al., 2012. World agriculture towards 2030/2050: the 2012 revision. ESA Working Paper No. 12-03.

Alexandridis, T., Cherif, I., Chemin, Y., Silleos, G., Stavrinos, E., Zalidis, G., 2009. Integrated methodology for estimating water use in Mediterranean agricultural areas. Remote Sens. 1, 445–465.

Allen, R.G., Pereira, L.S., Raes, D., Smith, M., 1998. Crop evapotranspiration—guidelines for computing crop water requirements. FAO Irrigation and Drainage Paper 56. FAO, Rome, Italy, p. 300. ⟨http://www.fao.org/docrep/x0490e/x0490e00.htm⟩ (Available at).

Allen, R.G., Tasumi, M., Trezza, R., 2007. Satellite-based energy balance for mapping evapotranspiration with internalized calibration (METRIC)—Model. J. Irrig. Drain. Eng. 133, 380–394.

Anderson, M.C., Kustas, W.P., Norman, J.M., Hain, C.R., Mecikalski, J.R., Schultz, L., Gonzalez-Dugo, M.P., Cammalleri, C., D'Urso, G., Pimstein, A., Gao, F., 2011. Mapping daily evapotranspiration at field to continental scales using geostationary and polar orbiting satellite imagery. Hydrol. Earth Syst. Sci. 15 (1), 223–239.

Anderson, M.C., Norman, J.M., Diak, G.R., Kustas, W.P., Mecikalski, J.R., 1997. A two-source time-integrated model for estimating surface fluxes using thermal infrared remote sensing. Remote Sens. Environ. 60, 195–216. https://doi.org/10.1016/S0034-4257(96)00215-5.

Barsi, J.A., Alhammoud, B., Czapla-Myers, J., Gascon, F., Haque, M.O., Kaewmanee, M., Markham, B.L., 2018. Sentinel-2A MSI and Landsat-8 OLI radiometric cross comparison over desert sites. Eur. J. Remote Sens. 51 (1), 822–837.

Bastiaanssen, W.G., Ali, S., 2003. A new crop yield forecasting model based on satellite measurements applied across the Indus Basin, Pakistan. Agric. Ecosyst. Environ. 94, 321–340.

Bastiaanssen, W.G., Menenti, M., Feddes, R., Holtslag, A., 1998. A remote sensing surface energy balance algorithm for land (SEBAL). 1. Formulation. J. Hydrol. 212, 198–212.
Bastiaanssen, W., Noordman, E., Pelgrum, H., Davids, G., Thoreson, B., Allen, R., 2005. SEBAL model with remotely sensed data to improve water-resources management under actual field conditions. J. Irrig. Drain. Eng. 131, 85–93.
Bittelli, M., Pellegrini, S., Olmi, R., Andrenelli, C., Simonetti, G., Borrelli, E., Morari, F., 2022. Experimental evidence of laser diffraction accuracy for particle size analysis. Geoderma 409, 115627.
Brisson, N., Gary, C., Justes, E., Roche, R., Mary, B., Ripoche, D., Sinoquet, H., 2003. An overview of the crop model STICS. Eur. J. Agron. 18 (3–4), 309–332. https://doi.org/10.1016/S1161-0301(02)00110-7.
Brutsaert, W., Sugita, M., 1992. Application of self-preservation in the diurnal evolution of the surface energy budget to determine daily evaporation. J. Geophys. Res. Atmos. 97, 18377–18382.
Calera Belmonte, A., Campos, I., Osann, A., D'Urso, G., Menenti, M., 2017. Remote Sens. for crop water management: from ET modelling to services for the end users. Sensors 17, 1104. https://doi.org/10.3390/s17051104.
Chastain, D.R., Snider, J.L., Collins, G.D., Perry, C.D., Whitaker, J., Byrd, S.A., Oosterhuis, D.M., Porter, W.M., 2016. Irrigation scheduling using predawn leaf water potential improves water productivity in drip-irrigated cotton. Crop Sci. 56, 3185–3195.
Chávez, J.L., Pierce, F.J., Elliott, T.V., Evans, R.G., Kim, Y., Iversen, W.M., 2010. A remote irrigation monitoring and control system (RIMCS) for continuous move systems. Part B: field testing and results. Precis. Agric. 11, 11–26.
Chen, Y., Zhang, Z., Tao, F., 2018. Improving regional winter wheat yield estimation through assimilation of phenology and leaf area index from remote sensing data. Eur. J. Agron. 101, 163–173. https://doi.org/10.1016/j.eja.2018.09.006.
Choudhury, B.J., 1987. Relationships between vegetation indices, radiation absorption, and net photosynthesis evaluated by a sensitivity analysis. Remote Sens. Environ. 22, 209–233.
Corbari, C., Charfi, I.B., Al Bitar, A., Skokovic, D., Sobrino, J.A., Perelli, C., Branca, G., Mancini, M., 2022. A fully coupled crop-water-energy balance model based on satellite data for maize and tomato crops yield estimates: the FEST-EWB-SAFY model. Agric. Water Manag. 272, 107850.
Corbari, C., Mancini, M., 2014. Calibration and validation of a distributed energy water balance model using satellite data of land surface temperature and ground discharge measurements. J. hydrometeor. 15, 376–392.
Corbari, C., Mancini, M., 2023. Irrigation efficiency optimization at multiple stakeholders' levels based on remote sensing data and energy water balance modelling. Irrig. Sci. 41, 121–139. https://doi.org/10.1007/s00271-022-00780-4.
Corbari, C., Ravazzani, G., Mancini, M., 2011. A distributed thermodynamic model for energy and mass balance computation: FEST-EWB. Hydrol. Process. 25, 1443–1452.
Corbari, C., Skokovic, D., Nardella, L., Sobrino, J., Mancini, M., 2020. Evapotranspiration estimates at high spatial and temporal resolutions from an energy–water balance model and satellite data in the capitanata irrigation consortium. Remote Sens 12, 4083. https://doi.org/10.3390/rs12244083.
D'Urso, G., 2010. Current status and perspectives for the estimation of crop water requirements from earth observation. Ital. J. Agron. 5, 107–120.
Duchemin, B., Maisongrande, P., Boulet, G., Benhadj, I., 2008. A simple algorithm for yield estimates: evaluation for semi-arid irrigated winter wheat monitored with green leaf area index. Environ. Modell. Softw. 23 (7), 876–892. https://doi.org/10.1016/j.envsoft.2007.10.003.
Duethmann, D., Anderson, M., Maneta, M.P., Tetzlaff, D., 2024. Improving process-consistency of an ecohydrological model through inclusion of spatial patterns of satellite-derived land surface temperature. J. Hydrol. 628, 130433.
Dyke, P.T., Kiniry, J.R., Jones, C.A., 1986. CERES-Maize: A Simulation Model of Maize Growth and Development. Texas A&M University Press, College Station. Retrieved from. http://catalog.hathitrust.org/Record/000810137.
Falkenberg, N.R., Picinni, G., Cothren, J.T., Leskovar, D.I., Rush, C.M., 2007. Remote sensing of biotic and abiotic stress for irrigation management of cotton. Agric. Water Manag. 87, 23–31.
FAO, 2018. The State of Food and Agriculture. Rome, Italy.
Fridgen, J.J., Kitchen, N.R., Sudduth, K.A., Drummond, S.T., Wiebold, W.J., Fraisse, C. W., 2004. Management zone analyst (MZA). Agron. J. 96, 100–108.
Gao, F., Anderson, M.C., Zhang, X., Yang, Z., Alfieri, J.G., Kustas, W.P., Mueller, R., Johnson, D.M., Prueger, J.H., 2017. Toward mapping crop progress at field scales through fusion of Landsat and MODIS imagery. Remote Sens. Environ. 188, 9–25.
Gobbo, S., Lo Presti, S., Martello, M., Panunzi, L., Berti, A., Morari, F., 2019. Integrating SEBAL with in-field crop water status measurement for precision irrigation applications—a case study. Remote Sens 11, 2069. https://doi.org/10.3390/rs11172069.
Grosso, C., Manoli, G., Martello, M., Chemin, Y.H., Pons, D.H., Teatini, P., Piccoli, I., Morari, F., 2018. Mapping maize evapotranspiration at field scale using SEBAL: a comparison with the FAO method and soil-plant model simulations. Remote Sens. 10 (9).
Gutman, G., Ignatov, A., 1998. The derivation of the green vegetation fraction from NOAA/AVHRR data for use in numerical weather prediction models. Int. J. Remote Sens. 19 (8), 1533–1543.
Guzinski, R., Nieto, H., 2019. Evaluating the feasibility of using Sentinel-2 and Sentinel-3 satellites for high-resolution evapotranspiration estimations. Remote Sens. Environ. 221, 157–172. https://doi.org/10.1016/j.rse.2018.11.019.
Ingram, J., 2011. A food systems approach to researching food security and its interactions with global environmental change. Food Secur 3, 417–431. https://doi.org/10.1007/s12571-011-0149-9.
Jashami, A., H., Nackley, L., Higgins, C., 2021. A variable rate drip irrigation prototype for precision irrigation. Agronomy 11 (12), 2493. https://doi.org/10.3390/agronomy11122493.
Jin, Z., Azzari, G., You, C., Di Tommaso, S., Aston, S., Burke, M., Lobell, D.B., 2019. Smallholder maize area and yield mapping at national scales with Google Earth Engine. Remote Sens. Environ. 228, 115–128. https://doi.org/10.1016/j.rse.2019.04.016.
Ke, Y., Im, J., Park, S., Gong, H., 2016. Downscaling of MODIS one kilometer evapotranspiration using Landsat-8 data and machine learning approaches. Remote Sens. 8, 215.
Knipper, K.R., Kustas, W.P., Anderson, M.C., Alfieri, J.G., Prueger, J.H., Hain, C., Gao, F. N., Yang, Y., McKee, L.G., Nieto, H., Hipps, L., Aisha, M., Sanchez, L., 2019. Evapotranspiration estimates derived using thermal-based satellite remote sensing and data fusion for irrigation management in California vineyards. Irrig. Sci. 37, 431–449. https://doi.org/10.1007/s00271-018-0591-y.
Koech, R., Langat, P., 2018. Improving irrigation water use efficiency: a review of advances, challenges and opportunities in the australian context. Water 10, 1771. https://doi.org/10.3390/w10121771.
Kustas, W.P., Li, F., Jackson, T.J., Pruger, J.H., MacPherson, J.I., Wolden, M., 2004. Effects of remote sensing pixel resolution on modeled energy flux variability of croplands in Iowa. Remote Sens. Environ. 92, 535–547. https://doi.org/10.1016/j.rse.2004.02.020.
Liakos, V., Porter, W., Liang, X., Tucker, M., McLendon, A., Vellidis, G., 2017. Dynamic variable rate irrigation—a tool for greatly improving water use efficiency. Adv. Anim. Biosci. 8, 557–563.
Li, X., Zhao, W., Li, J., Li, Y., 2018. Crop yield and water use efficiency as affected by different soil-based management methods for variable-rate irrigation in a semi-humid climate. Trans. ASABE 61 (6), 1915–1922. https://doi.org/10.13031/trans.13036.
Longo, M., Piccoli, I., Minasny, B., Morari, F., 2020. Soil apparent electrical conductivity-directed sampling design for advancing soil characterization in agricultural fields. Vadose Zo. J. 19, 1–14.
Lu, Y., Chibarabada, T.P., Ziliani, M.G., Kileshye Onema, J.-M., McCabe, M.F., Sheffield, J., 2021. Assimilation of soil moisture and canopy cover data improves maize simulation using an under-calibrated crop model. Agric. Water Manag. 252, 106884 https://doi.org/10.1016/j.agwat.2021.106884.
Meron, M., Tsipris, J., Orlov, V., Alchanatis, V., Cohen, Y., 2010. Crop water stress mapping for site-specific irrigation by thermal imagery and artificial reference surfaces. Precis. Agric. 11, 148–162.
Norman, J.M., Kustas, W.P., Humes, K.S., 1995. Source approach for estimating soil and vegetation energy fluxes in observations of directional radiometric surface temperature. Agric. Meteorol. 77 (3-4), 263–293.
Ortuani, B., Facchi, A., Mayer, A., Bianchi, D., Bianchi, A., Brancadoro, L., 2019. Assessing the effectiveness of variable-rate drip irrigation on water use efficiency in a vineyard in Northern Italy. Water 11 (10), 1964. https://doi.org/10.3390/w11101964.
O'Shaughnessy, S.A., Evett, S.R., Andrade, A., Workneh, F., Price, J.A., Rush, C.M., 2016. Site-specific variable-rate irrigation as a means to enhance water use efficiency. Trans. ASABE 59, 239–249.
O'Shaughnessy, S.A., Evett, S.R., Colaizzi, P.D., Andrade, M.A., Marek, T.H., Heeren, D. M., Lamm, F.R., LaRue, J.L., 2019. Identifying advantages and disadvantages of variable rate irrigation: an updated review. Appl. Eng. Agric. 35 (6), 837–852.
Paciolla, N., Corbari, C., Maltese, A., Ciraolo, G., Mancini, M., 2021. Proximal-sensing-powered modelling of energy-water fluxes in a vineyard: a spatial resolution analysis. Remote Sens. 13, 4699. https://doi.org/10.3390/rs13224699.
Papadavid, G., Hadjimitsis, D.G., Toulios, L., Michaelides, S., 2013. A modified SEBAL modeling approach for estimating crop evapotranspiration in semi-arid conditions. Water Resour. Manag. 27, 3493–3506.
Piccoli, I., Lazzaro, B., Furlan, L., Berti, A., Morari, F., 2021. Examining crop root apparatus traits in a maize-soybean-winter wheat rotation under conservation agriculture management. Eur. J. Agron. 122, 126171.
Skokovic, D., 2017. Calibration and Validation of Thermal Infrared Remote Sensing Sensors and Land/Sea Surface Temperature algorithms over the Iberian Peninsula (Ph.D. dissertation). Universidad de Valencia, Valencia, Spain.
Snider, J., Chastain, D., Porter, W., 2015. Plant-based irrigation scheduling. In: Snider, J., Oosterhuis, D. (Eds.), Linking Physiology to Management. The Cotton Foundation, Cordova, TN, USA.
Sobrino, J.A., Jiménez-Muñoz, J.C., Sòria, G., Ruescas, A.B., Danne, O., Brockmann, C., Ghent, D., Remedios, J., North, P., Merchant, C., Berger, M., Mathieu, P.P., Göttsche, F.-M., 2016. Synergistic use of MERIS and AATSR as a proxy for estimating Land Surface Temperature from Sentinel-3 data. Remote Sens. Environ. 179, 149–161.
Sobrino, J.A., Li, Z.L., Stoll, M.P., Becker, F., 1996. Multi-channel and multi-angle algorithms for estimating sea and land surface temperature with ATSR data. Int. J. Remote Sens. 17 (11), 2089–2114.
Sobrino, J.A., Skokovic, D., Jiménez-Muñoz, J.C., 2015. Spatial analysis of the homogeneity of the land Surface temperature in three Spanish test sites. Int. J. Remote Sens. 36, 4793–4807.
Su, Z., 2002. The surface energy balance system (SEBS) for estimation of turbulent heat fluxes. Hydrol. Earth Syst. Sci. 6, 85–100. https://doi.org/10.5194/hess-6-85-2002.
Sui, R., Yan, H., 2017. Field study of variable rate irrigation management in humid climates. Irrig. Drain. 66 (3), 327–339. https://doi.org/10.1002/ird.2111.
Teixeira, A.D.C., Bastiaanssen, W., Ahmad, M., Bos, M., 2009. Reviewing SEBAL input parameters for assessing evapotranspiration and water productivity for the low-middle Sao Francisco River basin, Brazil: Part A: calibration and validation. Agric. Meteorol. 149, 462–476.

Vazifedoust, M., Van Dam, J., Bastiaanssen, W., Feddes, R., 2009. Assimilation of satellite data into agrohydrological models to improve crop yield forecasts. Int. J. Remote Sens. 30, 2523–2545.

Vellidis, G., Liakos, V., Porter, W., Tucker, M., Liang, X., 2016. A dynamic variable rate irrigation control system. In Proceedings of the 13th International Conference on Precision Agriculture, St. Louis, MI, USA.

Vellidis, G., Tucker, M., Perry, C., Reckford, D., Butts, C., Henry, H., Liakos, V., Hill, R., Edwards, W., 2013. A soil moisture sensor-based variable rate irrigation scheduling system. Precision Agriculture'13. Springer, Berlin, Germany, pp. 713–720.

Vuolo, F., D'Urso, G., De Michele, C., Bianchi, B., Cutting, M., 2015. Satellite-based irrigation advisory services: a common tool for different experiences from Europe to Australia. Agric. Water Manag. 147, 82–95. https://doi.org/10.1016/j.agwat.2014.08.004.

Wada, Y., van Beek, L.P.H., Bierkens, M.F.P., 2011. Modelling global water stress of the recent past: on the relative importance of trends in water demand and climate variability. Hydrol. Earth Syst. Sci. 15, 3785–3808. https://doi.org/10.5194/hess-15-3785-2011.

Wang, J., Li, X., Lu, L., Fang, F., 2013. Estimating near future regional corn yields by integrating multi-source observations into a crop growth model. Eur. J. Agron. 49, 126–140. https://doi.org/10.1016/j.eja.2013.03.005.

Xue, J., Anderson, M.C., Gao, F., Hain, C., Knipper, K.R., Yang, Y., Kustas, W.P., Yang, Y., Bambach, N., McElrone, A.J., Castro, S.J., 2022. Improving the spatiotemporal resolution of remotely sensed ET information for water management through Landsat, Sentinel-2, ECOSTRESS and VIIRS data fusion. Irrig. Sci. 40 (4-5), 609–634.

Zhang, Z., Li, Z., Chen, Y., Zhang, L., Tao, F., 2020. Improving regional wheat yields estimations by multi-step-assimilating of a crop model with multi-source data. Agric. For. Meteor. 290, 107993 https://doi.org/10.1016/j.agrformet.2020.107993.

Zhang, Y., Schaap, M.G., 2017. Weighted recalibration of the rosetta pedotransfer model with improved estimates of hydraulic parameter distributions and summary statistics (Rosetta3). J. Hydrol. 547, 39–53.

Zhao, W., Li, J., Yang, R., Li, Y., 2017. Crop yield and water productivity responses in management zones for variable-rate irrigation based on available soil water holding capacity. Trans. ASABE 60 (5), 1659–1667. https://doi.org/10.13031/trans.12340.